



Capture efficiency of magnetic nanoparticles through the compaction effect of a microparticles column

K. B. Reynoso-Hernández , P. E. Guevara-Pantoja, and G. A. Caballero-Robledo 

CINVESTAV-Monterrey, PIIT, Nuevo León, 66600, México



(Received 10 March 2021; accepted 21 July 2021; published 13 August 2021)

When a magnetic nanoparticle solution flows through a porous medium formed by iron microparticles packed in a microfluidic channel, the nanoparticles get trapped within the column in the presence of a magnet. A complex interplay between magnetic and fluid forces within the magnetized porous medium governs the trapping of nanoparticles. However, how does the packing state of the microparticles affect the trapping of nanoparticles? Will more nanoparticles be trapped on a loose or a tight packing? In this work, we present experiments that show that the capture of nanoparticles is determined by the total volume occupied by the column, independent of its packing density. We present a simple analytical model based on the competition of drag and magnetic forces that shows that our system can be useful to develop and test more complete and accurate models. We also developed a technique to measure the columns' minute mass and its packing density, which consists of injecting polydimethylsiloxane into the acrylic microfluidic device. Our work can help with the optimization of environmental and biomedical applications based on high-gradient magnetic nanoparticle separation.

DOI: [10.1103/PhysRevE.104.024603](https://doi.org/10.1103/PhysRevE.104.024603)

I. INTRODUCTION

Magnetic nanoparticles (MNPs) are widely used in many industries and fields such as biomedicine and biotechnology [1]. Their fast and effective binding to biomolecules and their good dispersibility allow them to be used for biological separation [2–4], in drug delivery processes [5,6], and as immunosupport for immunoassays [7–11]. In biomedical applications, the large specific area of the MNPs and their Brownian motion allow them to capture more molecules per unit volume and more efficiently than conventional methods. These features reduce incubation times and increase detection sensitivity [12–14]. However, the large surface to volume ratio of MNPs favors drag and Brownian forces over magnetic forces. Therefore, high magnetic gradients are needed to capture them when immersed in a fluid [15–17]. This effect is so strong that particles smaller than 100 nm can only be captured if they are superparamagnetic, i.e., particles with no net magnetization but high magnetic susceptibility [18].

There have been different approaches to generate high magnetic gradients in microsystems. Some examples include placing a microstructure such as a microneedle or a microcomb [19], a ferromagnetic wire [20–22], or micropillar arrays [23–25].

A simple end efficient alternative to capture small superparamagnetic nanoparticles inside microfluidic channels was developed by Teste *et al.* [26]. It consists of a column of iron microparticles packed inside a polydimethylsiloxane (PDMS) channel. The microparticles act as individual magnets in the presence of an external magnetic field, generating strong magnetic gradients within the porous medium formed by the

packing. They studied the trapping efficiency for different flow rates, beads sizes, and permanent magnet positions. They showed that microparticles' presence in the channel enhances the magnetic force on nanoparticles by a factor of 10^3 . Then, the authors used the microfluidic magnetic trap to develop an allergy diagnosis immunoassay using the nanoparticles as immunosupport, improving the total time and the limit of detection of the test compared to a standard enzyme-linked immunosorbent assay (ELISA) test [27]. More recently, in our group, we developed a similar chip made from acrylic to perform detection of a model immunoassay [28]. These systems are ideal for developing point-of-care devices due to their simplicity. But, if a biomedical device based on a column of packed microparticles is to be produced massively, it is essential to optimize the system and assure reproducibility. Therefore, how should the microparticles be packed to optimize the capture of nanoparticles? Which will trap more nanoparticles, a loose or a compact packing?

In previous work, we showed that the column's packing density could be reversibly controlled by applying a vertical vibration protocol [29], similarly to what happens in dry macroscopic granular packings [30–32]. In this work, we went further by exploring the number of nanoparticles trapped in columns of different masses at different packing densities. In order to measure the columns' minute mass, we developed a technique which consists of extracting the microparticles column by injecting polydimethylsiloxane into the microfluidic channel.

We found that two columns of different densities but similar sizes capture the same amount of nanoparticles. This result means that, surprisingly, the packing density does not affect the capture. A simple analytical model based on competition between magnetism and fluid drag shows that our experimen-

*g.a.caballero.robledo@gmail.com

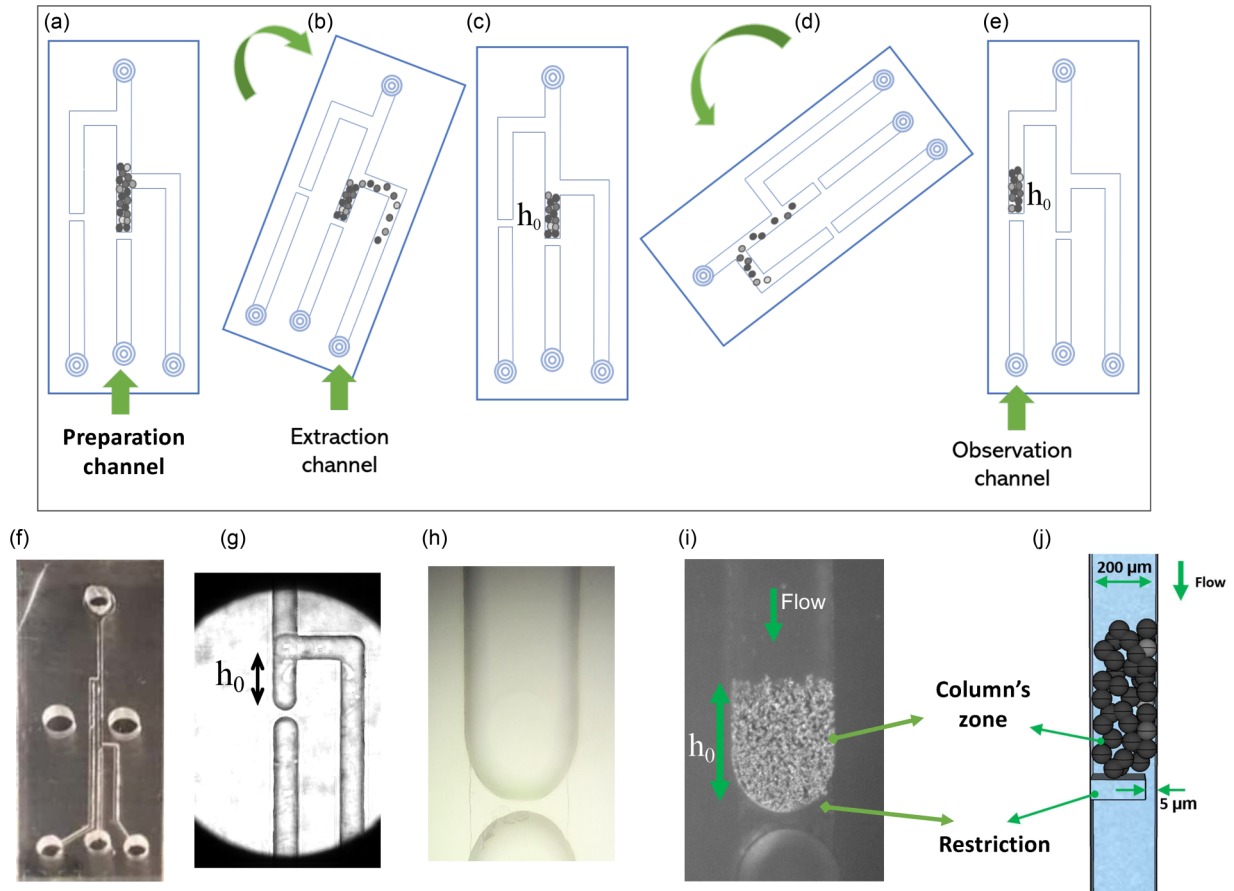


FIG. 1. [(a)–(e)] Schematic representation of the chip and the preparation protocol of columns of controlled height (and mass): (a) Microparticles are introduced into the preparation channel and fall by gravity up to the restriction. (b) The chip is tilted to the right for particles in excess to fall into the extraction channel. (c) A column of height h_0 rests in the preparation channel. (d) The microparticles pass to the observation channel by tilting the chip to the left. (e) The column of height h_0 in the observation channel is ready for an experiment. (f) Picture of the chip. (g) Closeup image of the preparation and extraction channels. (h) Image of the observation channel at the level of the restriction without microparticles. The width of the channel is $200\ \mu\text{m}$. (i) Front view of the observation channel with microparticles. h_0 is the initial height of the columns before vibration for compaction. (j) Schematic representation of a lateral view of the channel at the level of the restriction with particles: the $5\text{-}\mu\text{m}$ gap restriction lets fluid pass but not the particles.

tal setup can be an excellent system to develop and test more complete and accurate models.

II. EXPERIMENTAL SETUP

In this section, we present a brief description of the experimental setup, but more details of the materials and methods can be found in Appendix A.

Magnetic nanoparticles (MNPs) of $10\ \text{nm}$ in size were diluted in $200\ \text{ml}$ of a solution with a saline buffer and a surfactant which is commonly used to reduce nonspecific binding in immunoassays. Its use allows us to introduce and manipulate the microparticles inside the device, preventing them from adhering to the walls of the channels [33]. See Appendix A1 for details of the preparation of the solution of magnetic nanoparticles.

Carbonyl-iron microparticles ($8 \pm 1\ \mu\text{m}$) were coated by growing silica and silica-polyethylene glycol (PEG) layers on their surface to avoid adhesion and cohesion of nanoparticles. The procedure is described in detail in previous work by our group, where we show that the

functionalization reduces by 75% the number of nanoparticles that adhere to the microparticles without applying the magnetic field [28]. The density of the material that composes the microparticles is $\rho_{\mu p} = 7870\ \text{Kg/m}^3$. See Appendix A2 for details of the functionalization of iron microparticles.

The experimental setup consists of a microdevice that contains preparation, extraction, and observation channels [Figs. 1(a)–1(e)] on a $2\ \text{cm} \times 1.5\ \text{cm} \times 1.3\ \text{mm}$ acrylic piece, and sealed with another unprocessed piece of the same dimensions by exposing the acrylic to a mild solvent. The channels are carved on the acrylic sheet using a micromilling machine with a $200\text{-}\mu\text{m}$ square end-mill drill bit. The resulting milled channels are rough due to the fabrication process, but their roughness is smoothed when exposed to the solvent [34]. See Appendix A3 for details of microfabrication and chip bonding.

The channels have a $200 \times 200\ \mu\text{m}$ square cross section, except at restriction zones where the liquid passes but not the microparticles [see Figs. 1(i) and 1(j)]; there, the cross-section area is $200 \times 5\ \mu\text{m}$. Note that the channels' width is

determined by the size of the drill bit, while the depth depends on the penetration of the drill bit on the acrylic sheet, which is numerically controlled with the milling machine. However, the vertical displacements precision of the micromilling machine is not good enough to make the 5- μm deep restriction. To solve this problem, we built a home-made 3D-printed positioner fixture that uses cheap piezoelectric stacks to control the vertical position of the acrylic plate with a resolution of 500 nm and an accuracy of $\pm 1.5 \mu\text{m}$ [35].

The MNPs solution is injected into the channels through the top inlet using a syringe mounted on a syringe pump, and the flow is monitored at the exit with a flow sensor to maintain it at 10 $\mu\text{l/h}$ in all the experiments. This rate was chosen because it was observed that the increase in the packing density of a loose column due to flow is only of the order of 10%, compared to 20% for more massive flows (see Fig. S6 of the Supplemental Material [36]).

The chip's design allows us to reproducibly prepare columns of controlled mass and perform experiments of capture and release of magnetic nanoparticles. The chip is shown in Fig. 1. It consists of a column preparation channel where the microparticles are initially loaded with the chip in a vertical position. The microparticles fall rapidly through the channel because they are much denser than water. The channel has a 5- μm deep restriction that allows passing liquid but not microparticles. So, a column of microparticles is formed just above the restriction [Fig. 1(a)]. The column's mass is so small that it is difficult to load a controlled amount of particles into the chip. For this reason, we included an extraction channel connected to the preparation channel at a distance of h_0 from the restriction. The chip is then tilted to the right, forcing the particles that are above h_0 to fall into the extraction channel [Fig. 1(b)] and leaving a column of height h_0 in the preparation channel [Fig. 1(c)]. The vertical shaking of the device changes the compaction of the columns. Therefore, the experiments cannot be done in the preparation channel because the extraction channel would interfere with the microparticles' dynamics during the shaking. For this reason, we made an observation channel with a similar restriction and connected to the preparation channel at a point much higher than h_0 . By tilting the device to the left, the particles are transferred from the preparation channel to the observation channel [Fig. 1(d)]. The column formed in this way is in a loose state that corresponds to the initial state for the compaction and trapping experiments.

The column's packing density is controlled by a vertical vibration protocol that was previously reported by Guevara-Pantoja *et al.* [29]. Vibration is applied to the chip by placing it vertically on a base attached to a shaker that allows precise control of the amplitude and frequency (see Fig. S1 of the Supplemental Material [36] for a schematic representation of the experimental setup).

The packing density of a column is defined as

$$\rho = \frac{M_p}{Aw}, \quad (1)$$

where M_p is the total mass of the microparticles, A is the frontal area occupied by the column, and w is the depth of the channel. Since M_p and w are constant, it suffices to calculate A to obtain the packing density.

The vibration applied to the chip consists of a sinusoidal vertical shaking where the amplitude a and frequency f can be varied. The control parameter for the intensity of vibration is the normalized peak acceleration

$$\Gamma = \frac{a(2\pi f)^2}{g}, \quad (2)$$

where g is the acceleration of gravity. The vibration protocol used to vary the packing density of the column is the following: First, we measure the frontal area of the column of the initial state, A_0 . From Eq. (1), and considering that w and M_p are the same for all the columns, it follows that $\rho/\rho_0 = A_0/A$. Therefore, A_0 is used to normalize all the packing density states obtained throughout the vibration protocol. Afterward, the column is vibrated with acceleration Γ for 10 s, the vibration is stopped, the column settles down, and an image of the static column is recorded to determine the column's new volume. Then, vibration at different Γ is applied, and the process is repeated (Fig. S3 of the Supplemental Material [36] shows a column before, during, and after vibration). Γ is gradually increased up to $\Gamma = 30$ (ascending protocol) and then gradually reduced to 0 (descending protocol). See Appendix A4 for more details of the shaking and packing density variation.

A nearly constant magnetic field of magnitude $H_0 = 63\text{kA/m}$ can be applied to the column's zone by a horseshoe-shaped electromagnet designed by our group (see Fig. S9 of the Supplemental Material [36]). See Appendix A5 for more details of the applied magnetic field.

Using an electromagnet fixed in space allows turning the magnetic field on and off without disturbing the iron column. In contrast, if a permanent magnet is used, the column's grains move together with the magnet when it approaches and moves away, changing the configuration and compaction of the column [29].

The column's mass is of the order of micrograms and therefore it is difficult to measure with a conventional balance. For this purpose, we developed a protocol that allows us to extract the column of microparticles from the chip and measure their mass. See Appendix A6 for details of the protocol for extracting the mass.

The magnetic trap's efficiency to capture nanoparticles was studied as a function of the packing density of the microcolumns and for columns of different initial heights h_0 (i.e., columns of different mass).

First, the device is filled with MNPs solution, and the microparticle column is constructed, controlling its initial height of h_0 , and placed into the observation channel. Subsequently, the desired flow rate is established in the channel and a fluorescent image using a red filter and a 20 \times objective lens is taken downstream of the restriction to determine the fluorescence I_N that corresponds to the known concentration $C_N \approx 10^{14}$ MNP s/ml of the solution of MNPs. Then, the magnetic field is turned on, and the MNPs are trapped inside the porous medium formed by the iron microparticles. The saturation of the trap is reached after 7.5 min for the highest columns studied here. Then, the magnetic field is switched off, and the captured MNPs are released. Fluorescence images are taken downstream of the restriction at 15 frames per second during

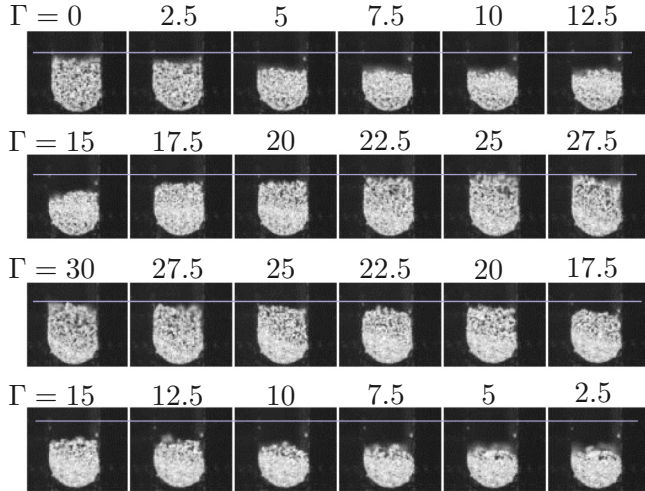


FIG. 2. Particles inside the channel through the vibration protocol: Γ increases gradually from 0 to 30 and back to 0. The initial packing density ρ_0 (upper left corner) is used to normalize all packing densities. The number of iron particles that compose the column is constant throughout the experiment. The horizontal line marks the initial height of h_0 . The width of the channel is $200 \mu\text{m}$.

the release of MNPs. Figure S11 of the Supplemental Material [36] shows a sequence of images during the liberation of nanoparticles from the trap. See Appendix A7 for details of the measurements of nanoparticle trapping.

III. RESULTS AND DISCUSSION

A. Varying the packing density by shaking

Figure 2 shows the packing density of a column of microparticles throughout the vibration protocol.

The value of the peak acceleration Γ [Eq. (2)] is varied by changing the amplitude a and keeping the frequency constant at $f = 650 \text{ Hz}$. First, the packing density increases together with Γ , but when the intensity of the shaking continues to increase, the column expands again, reaching the initial low packing density. Then, when Γ is reduced, the packing density increases until it reaches its maximum value, which corresponds to the most compact column. The packing density variation is remarkable, giving the impression that the mass of the column is changing, which is not the case. The particles that form the column are nonspherical and their size is polydisperse [28]; the nonsphericity favors loose packings while polydispersity favors compact packings. These features may explain the large density variations observed in our system.

B. Capture efficiency of magnetic nanoparticles

The magnetic trap's capture efficiency was studied by preparing columns of different initial heights, and therefore different masses, and gradually varying the columns' packing density, measuring at each stage of compaction the capacity of the columns to trap nanoparticles.

Figure 3 shows the number of trapped nanoparticles as a function of the columns' height. Empty symbols, indicated by a black arrow, represent the initial height of h_0 for each of the

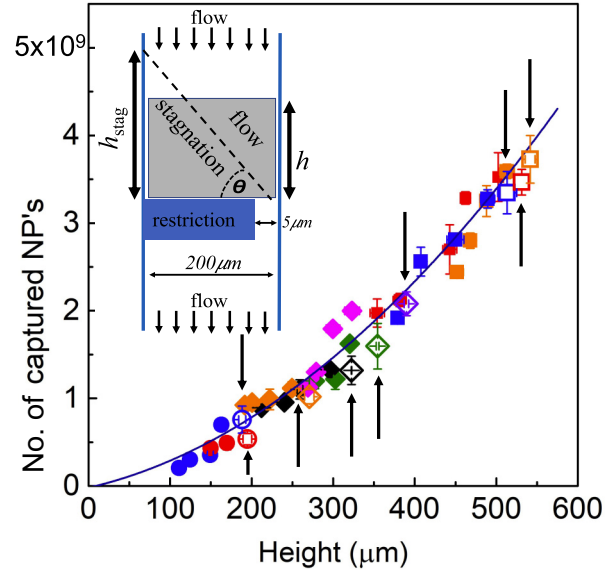


FIG. 3. Number of magnetic nanoparticles trapped in columns of different heights and compactions. Columns of different heights were prepared and then gradually compacted, measuring the trapped nanoparticles at each compaction stage. Empty symbols, pointed by a black arrow, represent the trapping in columns at their initial height h_0 , and full symbols of the same shape and color correspond to the same column but at different compactions. The curve is a quadratic function adjusted to the data. The inset represents the side view of the column (gray) and restriction (blue) to illustrate the idea of a zone of stagnation where no trapping occurs, which would be the cause of the quadratic relation.

columns analyzed. Full symbols of the same color and shape as the empty symbols correspond to the same column but at different compaction stages. Surprisingly, the data follow a nonlinear relation. This behavior is unexpected because, in principle, columns of different heights but with the same compaction should capture nanoparticles proportional to their height. If we assume that the columns that have just been prepared, and not shaken, have the same packing density, they should capture the same amount of nanoparticles per unit volume. Therefore, at least the open symbols in the figure should follow a linear relation, which is not observed.

We hypothesize that the underlying mechanism behind this behavior is the existence of a stagnation zone within the porous column, next to the restriction, where the flow is so small that the number of captured nanoparticles is negligibly small. The inset of Fig. 3 shows a schematic representation of the lateral view of the column and restriction zone with a simplified version of this stagnation zone, where the border between the flow and no-flow regions is a straight line that forms an angle θ with the restriction. Depending on the value of θ , h_{stag} can be either larger than, equal to, or smaller than the height h of the column. If we suppose that in the region of flow there is a capture capacity of s MNPs per unit volume, and that in the stagnation zone there is no trapping, it is straightforward to show that the total number n_{np} of trapped nanoparticles is

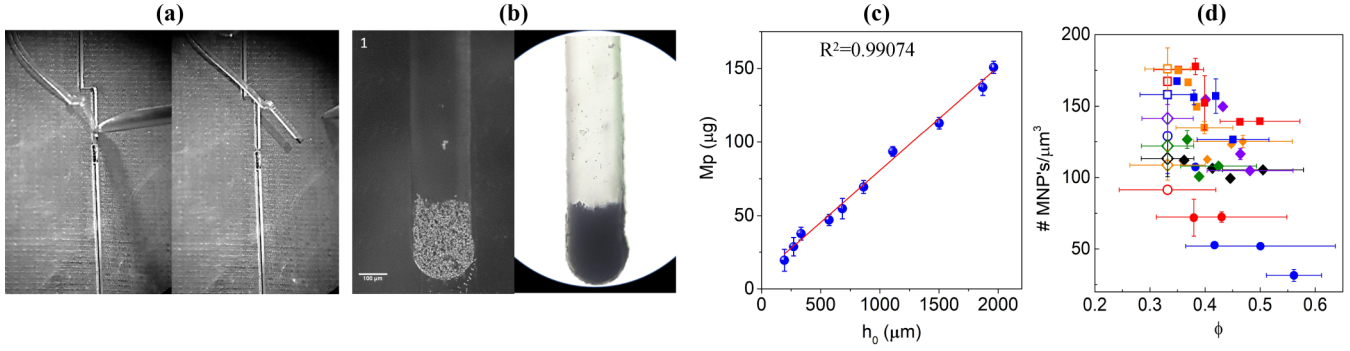


FIG. 4. (a) Images of the process of taking out the PDMS from the channel with a syringe's aid. (b) A column inside the channel and the same column within the polymerized PDMS outside the chip. (c) Mass measurements for columns of different initial heights h_0 , together with the linear regression to the data. (d) Number of trapped nanoparticles per unit volume as a function of the packing fraction. The symbols represent different columns. The open symbols indicate the initial state of the columns and correspond to the open symbols in Fig. 3. The packing fraction is obtained as explained after Eq. (4), where the mass is computed from the linear regression of the data in panel (c).

given by

$$n_{np} = \begin{cases} s \frac{1}{2} h_{\text{stag}} w^2 \left(\frac{h}{h_{\text{stag}}} \right)^2 & h \leq h_{\text{stag}}, \\ s \frac{1}{2} h_{\text{stag}} w^2 \left(2 \frac{h}{h_{\text{stag}}} - 1 \right) & h > h_{\text{stag}}, \end{cases} \quad (3)$$

where w is the width and depth of the square channel. Equation (3) predicts a quadratic relation for $h < h_{\text{stag}}$, and a transition to linearity when the height of the column becomes larger than h_{stag} . The continuum line in Fig. 3 is a quadratic fit to the data, which is an excellent fit. This suggests that the nonlinear behavior is indeed caused by the existence of a stagnation zone. We do not know the angle θ , but our data do not seem to transit to a linear relation, even for the highest columns. This result would indicate that the tiny gap of $5 \mu\text{m}$ of the restriction has a strong effect, creating a big stagnation zone. If that is the case, then a large share of the column's mass does not contribute to nanoparticles' trapping. This effect would undoubtedly be smaller if the channel's depth were reduced, but that would also increase the resistance of the whole system. Another solution to this problem would be to create spatially homogeneous restrictions, like a porous plug.

However, what is most striking in Fig. 3 is that the number of trapped nanoparticles of all the columns follows the same quadratic function, independently of their compaction. Indeed, two columns of the same height but very different compaction capture the same amount of nanoparticles. Compare, for example, the empty pink diamond at $h_0 \approx 390 \mu\text{m}$ and the blue full square at $h \approx 380 \mu\text{m}$. While the former is the most expanded state of that column, the latter is the most compact state of the column that initially had a height of $h_0 \approx 510 \mu\text{m}$. This comparison means that the number of trapped nanoparticles depends solely on the column's total volume and not on its compaction.

This behavior is surprising because it implies that the number of trapped nanoparticles per unit volume is the same for an expanded column with big pores and a compact column with small pores. Intuition suggests that these two situations would have different capacity to trap the nanoparticles. This result is also relevant for applications, like immunoassays [27,28], where the precise control of the number of trapped nanoparticles is essential to assure reproducibility.

C. Columns' mass

The images in Fig. 4(a) show the polymerized PDMS's extraction process from the channel with the aid of a syringe needle. In the image on the left, the needle is close to the zone of the restriction and the column. Figure 4(b) shows a column inside the channel and the same column outside the channel embedded in the PDMS strip. Figure 4(c) shows the mass of columns as a function of their height.

A linear regression to the data in Fig. 4(c) gives the relation

$$M_p = 9 \mu\text{g} + \left(7 \times 10^{-2} \frac{\mu\text{g}}{\mu\text{m}} \right) h_0. \quad (4)$$

With this relation, we are able to compute the total mass of the columns, where h_0 in Eq. (4) is the height of the columns represented by the open symbols in Fig. 3. Knowing the column's total mass allows us to estimate the packing fraction ϕ of the columns using Eq. (1) and the fact that $\rho = \rho_{\mu p} \phi$, where $\rho_{\mu p} = 7870 \text{ Kg/m}^3$ is the density of the material of the microparticles.

Figure 4(d) shows the number of trapped nanoparticles per unit volume as a function of the packing fraction. Notably, all the columns have the same packing fraction when they are in their initial state (open symbols), which means that our preparation method's reproducibility is excellent. Interestingly, one would have expected the number of trapped nanoparticles per unit volume to be constant, at least for columns of the same packing fraction. However, that is not the case due to the stagnation zone where no nanoparticles are trapped. Indeed, data in Fig. 4(d) are obtained by dividing the number of trapped nanoparticles by the total volume of the column. Therefore, the stagnation zone makes the effective density of trapped nanoparticles to be smaller for smaller columns. The same is true for a single column during the process of compaction: As a column becomes small, the relative size of the stagnation zone increases, and the density of nanoparticles trapped diminishes.

The fact that the total number of nanoparticles trapped is the same for columns of the same height, independent of their compaction, suggests that the number of trapped nanoparticles per unit volume is constant in the flow zone where the trapping happens. Assuming that our tallest columns are close to the

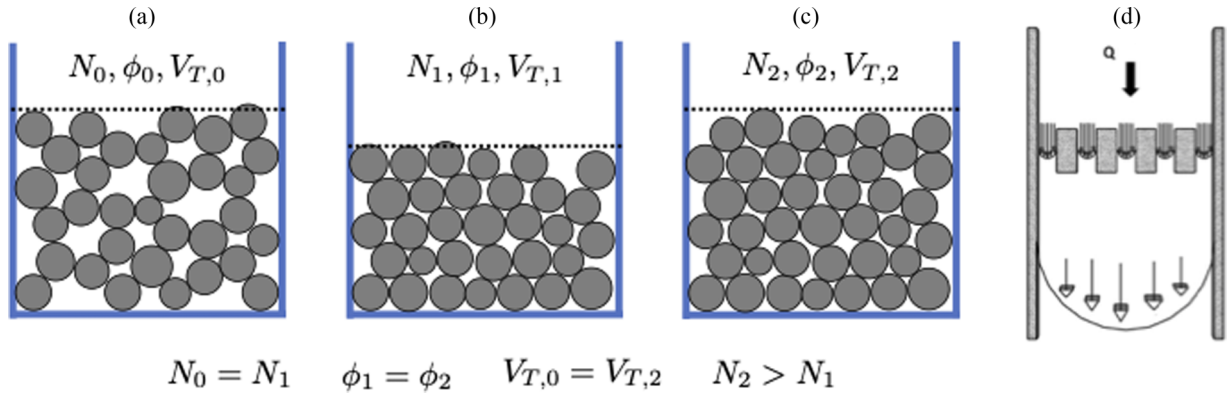


FIG. 5. (a) Schematic representation of an initial loose column with N_0 particles, packing density of ϕ_0 , and a total volume of $V_{T,0}$. (b) A compact column with the same number of particles as the column in panel (a) but with a packing density $\phi_1 > \phi_0$. (c) Column with the same packing density as column in panel (b), $\phi_2 = \phi_1$, occupying the same volume as column in panel (a), $V_{T,2} = V_{T,0}$, but with more particles than column (b), $N_2 > N_1$. (d) Representation of the porous medium as a set of equally sized cylindrical channels of radii R_i .

height of the stagnation zone h_{stag} , we estimate from Fig. 4(d) that the number of trapped nanoparticles per unit volume in the flow zone is of the order of $400 \text{ MNP s}/\mu\text{m}^3$.

Our method for extracting the columns from the chip embedded in PDMS proved useful to measure their minute mass and compute their packing fraction. This possibility is already precious, but this method has the potential to be used for other applications, for example, to process biological samples or capture molecules on the surface of the microparticles, and then have direct access to the microparticles for extra postprocessing.

IV. MODEL

How many nanoparticles n_{np} capture a column relative to the number of nanoparticles $n_{np,0}$ trapped by an initial, low-density packed column? We developed a very simple model, as a first approximation, to tackle this question. In this section, we present a brief description of the model, but the details can be found in Appendix B.

The trapping of nanoparticles inside the porous medium results from a complicated interplay of drag, magnetic, and Brownian forces. However, we found that the number of nanoparticles trapped in our system is susceptible to the flow velocity (see Fig. S15 of the Supplemental Material [36]), indicating that drag dominates over Brownian forces [15].

Our model assumes that trapping is determined by a competition between magnetic and drag forces on the nanoparticles inside the porous medium. The magnetic force on a nanoparticle depends on the magnetic gradients present inside the porous medium. Measuring or modeling these gradients in such a disordered medium is challenging. In contrast, it is simpler modeling the fluid flow inside the column as a function of its packing density.

The model is based on the assumption that, within each pore, the magnetic force will be larger than the drag force in regions where the flow velocity is below a critical value v_c . The nanoparticles would accumulate in these regions. This assumption is supported by a model of self-limited accumulation of colloids in porous media recently validated by Gerber *et al.* [37].

As a departure point, we oversimplify the system by doing three substantial assumptions: (1) The number of pores does not change with the packing density; (2) the accumulation of nanoparticles does not affect the flow of fluid in the pores; (3) the critical velocity does not change with the packing density.

The number of nanoparticles trapped per unit volume results from a competition between magnetic and drag forces. These competing forces change in a way that their effect cancels when the packing fraction varies, leaving the total number of trapped nanoparticles constant. Initially, our simple model did not capture this balance between effects [Eq. (B16)], predicting less trapping for a compact column than a loose column of the same height [Fig. 6(a)]. Then, we proposed a relation between the packing fraction and the critical velocity [Eq. (B17)] which manages to better reproduce the experimental results [Fig. 6(b)]. However, for the moment we do not have a justification for the proposed relation. Therefore, it is very likely that Eq. (B17) is incorrect, and that other factors must be taken into account, which would be the reason for the strange behavior observed for small columns of around $100 \mu\text{m}$ in Fig. 6(b). In particular, the gradual change of flow velocity in the pores as a consequence of the accumulation of nanoparticles is probably an important factor to consider [37]. It is noteworthy that the measurement of pressure changes in the microfluidic channel will give a lot of information in this regard through Darcy's law, which is something that we are planning for future experiments.

More evidence is needed to elaborate a more accurate model, but our experimental system proves to be an ideal setup to test models and advance the understanding of nanoparticles' magnetic capture inside a porous medium.

V. CONCLUSIONS

We have set up a well-controlled experiment that allows us to vary the packing density of micrometric columns of different masses and heights in the presence of flow and magnetic field.

This setup allowed us to study the capture of magnetic nanoparticles within the porous medium as a function of the volume occupied by the columns and independent of the pack-

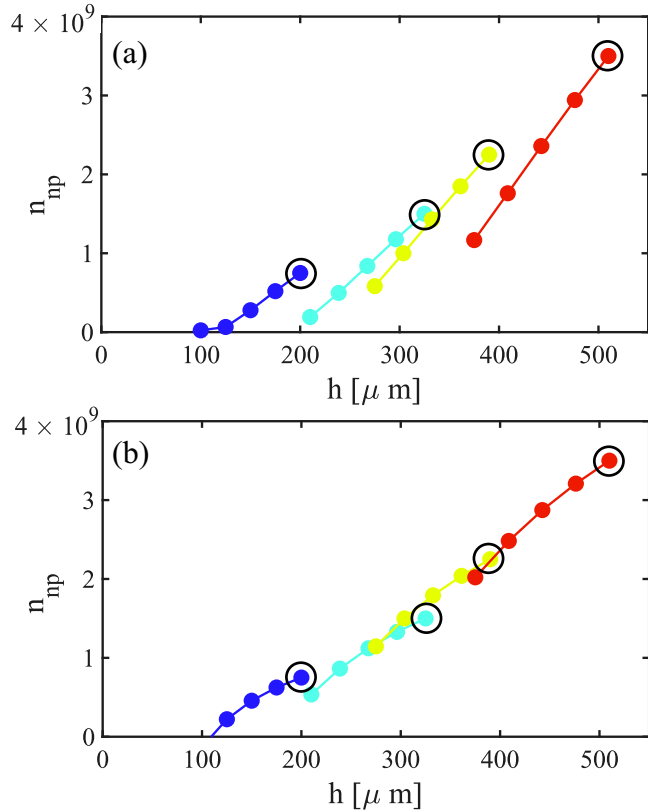


FIG. 6. To test the model we take the experimental values h_0 and $n_{np,0}$ of four columns (the points are indicated by the black circles) and we let h to reach its experimental final height in five steps. We calculate n_{np} predicted by Eq. (B16) [plotted in panel (a)] and by Eq. (B19) [plotted in panel (b)].

ing density. Surprisingly, the total number of nanoparticles captured depends solely on the column's volume, not on the packing density. Therefore, two columns of the same size, one very loose and another very compact, will capture the same amount of nanoparticles.

The capture of magnetic nanoparticles within a disordered porous medium is governed by the simultaneous action of drag, Brownian, electrostatic, and magnetic forces. Surface functionalization of the chip and particles, minimized the electrostatic interactions. Besides, we found that nanoparticles' capture is very sensitive to the flow rate, which indicates that Brownian forces on nanoparticles are not relevant. We thus propose a simple model based on the competition of drag and magnetic forces. The model manages to reproduce the experimental results, but only if we assume a specific functional relationship between the packing density and the critical capture velocity. For the moment, we cannot justify this functional relation, and more experimental evidence is needed to understand the complex mechanisms governing the capture of magnetic nanoparticles inside a magnetic porous medium. However, our experimental set up has proved to be an excellent system to develop and test future models.

The fabrication in acrylic by micromilling is relatively cheap and easy to implement. In contrast, the fabrication technique forced us to design an asymmetric restriction, which,

combined with the small gap needed to avoid the passage of microparticles, resulted in a non-negligible stagnation zone where nanoparticles are not captured. This stagnation zone seems to be much larger than what we had expected, meaning that a large share of the columns' mass does not contribute to the capture of nanoparticles. Nevertheless, we do not have direct evidence of this stagnation zone's existence and properties, so it would be interesting to study it, putting special attention to its behavior as a function of packing density. A homogeneous restriction, like a porous membrane, would avoid forming a stagnation zone and improve the capture efficiency of the magnetic trap.

Embedding the column in a polymer, "freezing" its structure, and having direct access to it by extracting it from the chip is a method that we believe can be useful for several applications. Here, it allowed us to measure the columns' mass, but it could be useful to study the structure of the granular packing as a function of compaction without the need to make x-ray tomography. This technique could also be used to access molecules or cells captured on the microparticles' surface for postprocessing.

The motivation to study this system comes from the use of the magnetic trap to perform immunoassays. High-gradient magnetic separation, combined with microfluidics, has proved to reduce assay time and sample volume, and our group has been able to perform tests with an excellent limit of detection. Besides, our chips are made of acrylic, which is a thermoplastic compatible with mass production. These features make these chips suitable to be used as point-of-care devices. However, for such applications, good reproducibility is obliged. Therefore, understanding and controlling the capture of nanoparticles is crucial. In this context, knowing that the number of nanoparticles trapped depends solely on the total volume of the column is important, and we are sure that it will be useful for other applications.

ACKNOWLEDGMENTS

The authors thank, J. C. Ruiz-Suárez, J. L. García-Cordero, and J. Carrillo for technical support and fruitful discussions. This work has been supported by Conacyt, Mexico, under Grant Fronteras de la Ciencia No. FC-2015-2/1178. K.B.R.-H. thanks Conacyt for financial support.

APPENDIX A: MATERIALS AND METHODS

1. Preparation of the solution of magnetic nanoparticles

Magnetic nanoparticles (MNPs) of 10 nm in size (rhodamine B iron nanoparticles, Ocean Nanotech, IRB-10-02) were diluted in 200 ml of ultrapure water from a Milli-Q Biocel system, a tablet of phosphate-buffered saline (PBS, Sigma Aldrich, Sigma-Aldrich, p4417), and Tween 20 (polyoxyethylene sorbitan monolaurate, Sigma-Aldrich, P1379) at 0.1%. Figure S2 of the Supplemental Material [36] shows the effect of using this solution on preventing the adhesion of microparticles to the channels.

2. Functionalization of iron microparticles

Bare carbonyl-iron microparticles ($8 \pm 1 \mu m$, 44890, Sigma-Aldrich, USA) were coated by growing silica and

silica-PEG layers on their surface [28]. Briefly, 1g of particles were mixed in a vial with 5ml of ethanol (459844, Sigma-Aldrich, USA), 1ml of tetraethyl orthosilicate (TEOS, 86578, Sigma-Aldrich, USA), and 250 μ l of ammonium hydroxide (NH₃OH, 320 145, Sigma-Aldrich, USA). The vial with the mix was agitated for 2 h, and the microparticles were washed with ethanol three times. Afterward, 5ml of ethanol, 500 μ l of PEG-APTES (PSIM6492, Gelest Inc., USA), and 250 μ l of NH₃OH were added to the vial, and it was agitated for 1.5 h. Subsequently, 500 μ L of TEOS was added, and the mix was agitated for 12h. As a final step, the microparticles were washed with ethanol, and they were let to dry at ambient temperature.

3. Microfabrication and chip bounding

The microfluidic devices were fabricated using 2 cm \times 1.5 cm \times 1.3 mm acrylic (poly(methyl methacrylate), Goodfellow, ME303018) sheets. The channels are carved on one acrylic sheet using a computer numerical control (CNC) micromilling machine (Roland MDX-40A) using a 200- μ m square end-mill drill bit (Kyocera, 1600-0080L012) at a spindle speed of 15 000 rpm and a feed rate of 1 mm/s. The carved sheet is sealed with another unprocessed piece of the same dimensions. Smooth channels can be obtained by sealing the device through chloroform exposure [38] while using a mild solvent at the sealing process makes rough channels. However, when we compared the response of the microcolumn packing density for smooth and rough channels, we observed better initial fluidization, higher initial compaction, and in general better control of the packing density when using rough channels (see Fig. S7 of the Supplemental Material [36]). The channels' roughness increases the friction between the channels and the microparticles, improving the transfer of energy to the granular material and allowing a more expanded building supported by the channels' walls. Consequently, we decided to make the experiments of this work using rough channels.

The sealing method based on a mild solvent for our devices was adapted from Brown *et al.* [39]: a mild solvent is made by mixing 47.5% of dimethylsulfoxide (DMSO, Sigma-Aldrich, D4540), 5% of methanol (Sigma-Aldrich, 322415), and 47.5% of ultrapure water. A drop of the solvent is poured between the acrylic pieces, and they are placed facing each other in a homemade mechanical press for 8 min at 98 °C and 72.5 psi. The glass transition temperature of our acrylic is above 100 °C [40].

Once the chip is sealed, we attach outer tubes (Tygon, ND-100.80, i.d. 0.02 in., o.d. 0.06 in.) to the inlets and outlets using instant glue (Loctite 945).

The MNPs solution is injected into the channels using a 100- μ l syringe (Hamilton 1710RNR) mounted on a syringe pump (Kdsscientific KDS-230), and the flow is monitored with a flow sensor (Flow Unit M for water, Fluigent).

4. Varying the packing density by vertically shaking

Vibration is applied using a permanent magnet shaker (LDS V201) controlled by a function generator (NI Elvis II, National Instruments). The column is imaged in its vertical

position with a microscope Nikon Eclipse TS100, which is turned 90 deg from its original orientation to focus on the vertical chip. A 20 \times objective lens is used with white light-emitting diodes adapted around it to observe the sample by reflecting light, and a color CCD camera (IDS UI-2230SE) is adapted to the microscope to record images like the one shown in Figs. 1(g)–1(i).

To calculate the packing density, it suffices to measure the frontal area A of a column. We use the open-source software IMAGEJ to calculate A by binarizing the frontal images. Nevertheless, the images are focused on the frontal grains, so the grains that are not in this plane are out of focus, making it difficult to precisely determine the correct binarization threshold value and, consequently, the packing density of the column. Therefore, we determined the evident extreme low and high values of the binarization threshold, obtaining the maximum and minimum possible values of the area occupied by the grains (Fig. S5 of the Supplemental Material [36] shows an example of the determination of the volume occupied by a column). The method for determining the column's volume from frontal images assumes that the column's upper surface is approximately flat. We verified that our vibration protocol produces columns with flat surfaces by observing a column from a side angle by cutting and polishing the device just next to the channel. Figure S3 of the Supplemental Material [36] shows a column with a flat surface before and after vibration observed from a lateral view.

The variations of Γ were done changing the amplitude a at a fixed frequency f in Eq. (2). However, to find the frequency's optimal value, we first studied the packing density behavior at different frequencies (Fig. S4 of the Supplemental Material [36]). We then chose the optimal frequency to perform the rest of the experiments. We also carried out experiments to verify the column's packing density control in presence of flow and magnetic field (Fig. S8 of the Supplemental Material [36]).

5. Magnetic field

A magnetic field can be applied to the column's zone by a horseshoe-shaped electromagnet designed by our group (see Fig. S9 of the Supplemental Material [36]). A direct current power supply of 2 A generates a nearly constant magnetic field of magnitude $H_0 = 63$ kA/m in the column's zone. The magnetic field was directly measured with a Gaussmeter.

The electromagnet needs to be water cooled due to the high current needed to generate the magnetic field. The cooling is done by putting it inside a small box connected to a circulating water system (LCB-R08, LabTech), which allows applying a flow rate of 2ml/s at a temperature of 22 °C.

The horseshoe's extremes cannot be inserted directly into the chip because they heat up the chip, and fluorescent signals are susceptible to temperature [41]. Instead, we insert into the chip two steel cylinders of 1.8 mm in diameter and 1.5 mm high to homogenize the field at the level of the restrictions [Fig. 1(f) shows the holes for the cylinders], and we place the electromagnet with the extremes of the horseshoe next to the cylinders, separated only by the 100- μ m-thick aluminum wall of the cooling box.

6. Measuring the mass of the columns

A polydimethylsiloxane prepolymer (PDMS, SYLGARD 184, 761036, Sigma Aldrich) is prepared by mixing a silicone elastomer base with a curing agent (cross linker, SYLGARD 184, 761028, Sigma Aldrich) in a 10:1 ratio, and it is kept in a simple vacuum hood (Nalgene Desiccator, 5310-0250, Thermo Scientific) for 30 min to eliminate air bubbles formed during mixing. Then, the mixture is injected into the column's microchannel, displacing the solution of MNPs without altering the column's structure. Afterward, to polymerize the mixture, the device is placed on a plate at 90°C for 3 h. Subsequently, the device is opened by detaching the faces of the chip, and the polymerized PDMS fragment is detached from the channel with the help of a syringe needle (see Fig. S10 of the Supplemental Material [36]).

Following the same procedure, a channel without microparticles is used to obtain a PDMS fragment as a reference. The masses of two segments of PDMS of the same length, one with and one without microparticles, are measured in an ultra-precise microbalance (Kibron Super G, Ultramicrobalance). The mass of the column of microparticles is the difference between the mass of the two segments. The columns are prepared as usual, and they are not vibrated; therefore, they have all the same packing density ρ_0 and their height is what we define as h_0 .

The use of PDMS strips to measure the mass is necessary because extracting and handling the particles out of the chip is not possible in our system without having a significant loss of particles. Another option would be to compare the chip's weight with and without particles, but the weight of a chip is larger than the maximum limit of the microbalance. In contrast, PDMS allows the extraction of the particles while the weight of the PDMS strips is still within the range of the microbalance.

Equation (4) shows that a systematic error in our measurements overestimates the mass of the columns by 9 μg , so we subtract this quantity for the calculation of the packing fraction.

7. Trapping efficiency of magnetic nanoparticles

The number of released nanoparticles is estimated by measuring the fluorescence intensity in a zone with a shape that takes into account the velocity profile of the flow and the time between frames to be sure that the measured signal on each frame does not count nanoparticles already counted on previous frames, and that there are no nanoparticles that cross this zone without being counted. The number of nanoparticles $n\text{MNP}_s(t)$ contained in the measurement zone at time t is computed using the relation

$$n\text{MNP}_s(t) = n\text{MNP}_{sC_N} \frac{I(t) - I_0}{I_N - I_0}, \quad (\text{A1})$$

where I_0 is the basal fluorescence of the chip and corresponds to the fluorescence of the channel filled with water, and $n\text{MNP}_{sC_N}$ is the number of nanoparticles contained in the measurement zone at the MNPs' concentration C_N of the injected solution. The total number of released nanoparticles is obtained from integrating $n\text{MNP}_s(t)$.

This method to count the number of particles is not exact because the parabolic velocity profile considered for the determination of the measurement zone corresponds to the plane at mid-depth of the channel, and it is assumed that the profile is the same at every other plane, which is inexact because it is a three-dimensional flow. Therefore, our computation slightly overestimates the number of nanoparticles, but this is a systematic error that does not affect the comparison of fluorescent intensity between experiments.

When the electromagnet is turned on, the nanoparticles flowing through the porous column get trapped there. During that time, the intensity of fluorescence diminishes in the channel after the restriction. After some time, the trap saturates of nanoparticles, and it cannot trap anymore. When this happens, the fluorescence intensity of the original solution of nanoparticles is recovered after the restriction. The time for saturation depends on the columns' size, but we observed that the saturation was reached after 7.5 min for our highest columns, so we used this time for trapping nanoparticles in all our experiments.

When the electromagnet is turned off, the trapped nanoparticles are released. By analyzing the fluorescence after the restriction, it is possible to quantify the number of released nanoparticles. Figure S11 of the Supplemental Material [36] shows an example of a release of nanoparticles after turning off the electromagnet, together with the fluorescence behavior as a function of time that results from image analysis. The process of capturing and releasing nanoparticles can be repeated consecutively on the same column with a remarkable degree of reproducibility (see Fig. S12 of the Supplemental Material [36]). The total number of nanoparticles released is obtained from integrating the fluorescence curves as a function of time.

APPENDIX B: NANOPARTICLES TRAPPING MODEL

The packing fraction ϕ is defined as

$$\phi = \frac{V_s}{V_T}, \quad (\text{B1})$$

where V_s is the volume occupied by the solid material of the microparticles and V_T is the total volume of the column. The relation between the packing density [Eq. (1)] and the packing fraction is $\rho = \rho_{\mu p} \phi$, where $\rho_{\mu p}$ is the density of the material of the microparticles.

We begin by considering columns in three different situations (Fig. 5): column 0 with low packing density ϕ_0 , with N_0 microparticles occupying a total volume $V_{T,0}$. Then, column 1 with the same number of particles, $N_1 = N_0$, but occupying a total volume $V_{T,1} < V_{T,0}$, which implies that $\phi_1 > \phi_0$. Finally, column 2 has the same packing density as column 1, $\phi_2 = \phi_1$, but occupies the same volume as column 0, $V_{T,2} = V_{T,0}$. Therefore, column 1 must have more particles than column 0, $N_2 > N_0$.

Packing fraction can be written as an expression of the total number of microparticles N , the volume of a single microparticle $V_{\mu p}$, and the void volume V_v , which is usually referred as the porosity of the column. But it can also be written in terms of h , the total mass of the column (M_p), and the cross-sectional

area of the microchannel A_c as follows:

$$\phi = \frac{NV_{\mu p}}{NV_{\mu p} + V_v} = \frac{M_p}{\rho_{\mu p} A_c} \left(\frac{1}{h} \right). \quad (\text{B2})$$

The porous medium formed by the disordered microparticles has a complex geometry. However, we will model it in a simplified way, assuming that each medium's pore is a cylinder. Moreover, we will assume that all the pores have the same cross-sectional area, A_i , and radius R_i . The resulting idealized porous medium is represented in Fig. 5(d). A flow Q is considered to flow through the channel and, for continuity, the same flow must pass through the porous medium. If the porous medium has N_{pores} in any cross section, then the flow in each channel would be

$$Q = \sum_i^{N_{\text{pores}}} Q_i = N_{\text{pores}} Q_i. \quad (\text{B3})$$

Similarly, the total void area of the cross-sectional area is

$$A_v = \sum_i^{N_{\text{pores}}} A_i = N_{\text{pores}} A_i = N_{\text{pores}} \pi R_i^2. \quad (\text{B4})$$

Writing the void area in terms of packing fraction, we can express

$$R_i^2 = \frac{A_c(1 - \phi)}{\pi N_{\text{pores}}}. \quad (\text{B5})$$

Now, we make one of the most substantial assumptions of the model. We will suppose that when the compaction of a column changes, the number of pores remains constant, and it is the size of the pores that change. This assumption is obviously not true, but it is probably a good approximation if we consider that when new contacts are formed in a granular material when the packing density increases, the particles that form the new contacts are initially not very far away from each other; it suffices that small displacements of particles have a relevant variation in packing fraction [42]. Besides, the no-slip condition at grains' surfaces suggests that such minute displacements would not significantly alter the flow. In contrast, these small displacements could be significant for the magnetic gradients within the porous medium.

If the number of pores remains constant, Eq. (B3) implies that the flow Q_i on each pore is also constant when ϕ changes. But if Q_i remains constant and R_i decreases, and if we assume a Poiseuille flow, then the flow velocity must increase following the relation

$$v_i^{\max} = \frac{2Q_i}{\pi R_i^2}, \quad (\text{B6})$$

where v_i^{\max} is the maximum velocity in the pore, and the expression for the corresponding parabolic velocity profile would be

$$v_i = v_i^{\max} \left(1 - \frac{r_i^2}{R_i^2} \right). \quad (\text{B7})$$

We expect that, within each pore, the strength of the magnetic force on nanoparticles is such that it is stronger than the drag force if the flow velocity is lower than a critical value v_c . This critical velocity defines a critical radius R_c for

which the region of the pore between R_c and R_i would then be filled with nanoparticles (see Fig. S14 of the Supplemental Material [36]).

Now, we would like to know how does the amount of trapped nanoparticles change when the packing density of the column changes. Another simplification that we make here is to consider that the velocity profile is not modified by accumulating nanoparticles. Following our experimental procedure, we express the number of trapped nanoparticles relative to the nanoparticles that trap an initial column with the lowest possible packing density ϕ_0 . Thus, any other column will have a larger packing density, $\phi > \phi_0$. We therefore define the adimensional quantities

$$\tilde{v}_i \equiv \frac{v_i}{v_{i,0}^{\max}}; \quad \tilde{v}_i^{\max} \equiv \frac{v_i^{\max}}{v_{i,0}^{\max}}; \quad \tilde{r}_i \equiv \frac{r_i}{R_{i,0}}; \quad \tilde{R}_i \equiv \frac{R_i}{R_{i,0}}, \quad (\text{B8})$$

where the subscript 0 refers to quantities associated to the initial expanded column. With these definitions we can write the adimensional form of the velocity profile inside the pores as

$$\tilde{v}_i = \tilde{v}_i^{\max} \left(1 - \frac{\tilde{r}_i^2}{\tilde{R}_i^2} \right). \quad (\text{B9})$$

Equation (B5) gives the relation between the size of the pores R_i and the packing density ϕ . Combining Eq. (B5) with Eqs. (B6), (B8), and (B9), it is possible to write \tilde{R}_i , \tilde{v}_i^{\max} , and \tilde{v}_i in terms of the packing density ϕ . A given critical velocity v_c determines different critical radius R_c for different packing densities (see Fig. S14 of the Supplemental Material [36]). The area occupied by nanoparticles A_{np} is determined by the interval between R_c and R_i (see Fig. S14(a) of the Supplemental Material [36]), and it is given by

$$A_{\text{np}} = \pi (R_i^2 - R_{i,c}^2) = \pi R_{i,0}^2 (\tilde{R}_i^2 - \tilde{R}_{i,c}^2). \quad (\text{B10})$$

Substituting in this equation an expression for the critical radius $\tilde{R}_{i,c}$ in terms of the critical velocity obtained from Eq. (B9) gives

$$\frac{A_{\text{np}}}{\pi R_{i,0}^2} = \tilde{R}_i^2 - \tilde{R}_i^2 \left(1 - \frac{\tilde{v}_{i,c}}{\tilde{v}_i^{\max}} \right) = \tilde{R}_i^2 \frac{\tilde{v}_{i,c}}{\tilde{v}_i^{\max}}, \quad (\text{B11})$$

where we have normalized A_{np} by the total area of a pore of the initial loose column.

The critical velocity v_c depends on the magnetic field and the particles' magnetic properties. For simplicity, we will assume for the moment that the critical velocity does not change with the packing density, which is certainly not true. We express the critical velocity as a fraction ϵ of the initial maximum velocity

$$v_{i,c} = \epsilon v_{i,0}^{\max}, \quad 0 \leq \epsilon \leq 1. \quad (\text{B12})$$

Therefore, from Eqs. (B8),

$$\tilde{v}_{i,c} = \epsilon. \quad (\text{B13})$$

Now, from the expressions of \tilde{R}_i and \tilde{v}_i^{\max} in terms of packing fraction and Eqs. (B11) and (B13), we can write

$$\frac{A_{\text{np}}}{\pi R_{i,0}^2} = \tilde{R}_i^2 \frac{\epsilon}{\tilde{v}_i^{\max}} = \left(\frac{1 - \phi}{1 - \phi_0} \right)^2 \epsilon. \quad (\text{B14})$$

If we substitute $\phi = \phi_0$ in Eq. (B14), we get $A_{\text{np},0} = \pi R_{i,0}^2 \epsilon$ and we obtain an expression for the variation of the captured nanoparticles as a function of the packing density

$$\frac{A_{\text{np}}}{A_{\text{np},0}} = \left(\frac{1 - \phi}{1 - \phi_0} \right)^2 = \left(\frac{\frac{1}{\phi_0} - \frac{\phi}{\phi_0}}{\frac{1}{\phi_0} - 1} \right)^2. \quad (\text{B15})$$

In our experiments, we measure the height h of the column and not the packing density. Thus, we would like to express Eq. (B15) in terms of h by means of the packing density shown in Eq. (B2). Since the ratio of the areas $A_{\text{np}}/A_{\text{np},0}$ is equal to the ratio of the volumes $V_{\text{np}}/V_{\text{np},0}$ and is also equal to the ratio of the number of trapped nanoparticles $n_{\text{np}}/n_{\text{np},0}$, we can obtain

$$n_{\text{np}} = \frac{\left(\frac{1}{\phi_0} - \frac{h_0}{h} \right)^2}{\left(\frac{1}{\phi_0} - 1 \right)^2} n_{\text{np},0}. \quad (\text{B16})$$

This is the relation that we were looking for: the variation of trapped nanoparticles as a function of the height of the column (which we measure in our experiments) and as a function of the initial packing density (which is well controlled with our experimental protocol). This expression allows us to compare the model with our experimental results directly.

To test the model, we generate four different typical initial columns based on the experimental results. For each column, we specify the initial height h_0 and the corresponding experimental initial number of trapped nanoparticles $n_{\text{np},0}$. We also specify the column's final height, and we make each column vary from the initial to the final height in five steps, which is a typical situation in our experimental data. Figure 6(a) shows the results of applying Eq. (B16) to the generated columns. It can be observed that the captured nanoparticles' behavior is different from what is observed in the experiments. The model predicts that two columns of the same height but different packing densities will capture nanoparticles differently: more trapping for lower density. In contrast, the experiments show that the amount of trapped nanoparticles depends solely on the column's total volume, independently of its packing density. Noteworthy, before doing our experiments, we hypothesized a behavior similar to what the model predicts, but the experiments showed we were wrong.

The discrepancy between our model and the experiments shows that we oversimplified the model with one or more

of our numerous assumptions. The three most substantial assumptions that we consider are the following: (1) The number of pores does not change with the packing density, (2) the accumulation of nanoparticles does not affect the flow of fluid in the pores; and (3) the critical velocity does not change with the packing density. With our experimental resources, it is not easy to assess the degree of validity of these assumptions. However, we believe that the magnetic gradients may be very sensitive to small displacements of the grains. For the moment, we do not have a model for the relation between the packing fraction and the critical velocity. Nevertheless, qualitatively we expect the magnetic gradients to be stronger around the microparticles if they are closer to each other, making the critical velocity larger if the packing density increases. We arbitrarily propose the simple relation

$$\tilde{v}_{i,c} = \epsilon = \left(\frac{1 - \phi_0}{1 - \phi} \right). \quad (\text{B17})$$

Equation (B14) would then take the form

$$\frac{A_{\text{np}}}{\pi R_{i,0}^2} = \left(\frac{1 - \phi}{1 - \phi_0} \right), \quad (\text{B18})$$

and this would lead to

$$n_{\text{np}} = \frac{\left(\frac{1}{\phi_0} - \frac{h_0}{h} \right)}{\left(\frac{1}{\phi_0} - 1 \right)} n_{\text{np},0}. \quad (\text{B19})$$

Figure 6(b) shows the result of applying Eq. (B19) to the same columns previously generated. This time, the behavior is similar as in experiments, i.e., the amount of nanoparticles trapped depends only on the column's total volume and not on the packing density.

Notably, the model aims to explain that two columns of the same height but different packing densities capture the same amount of nanoparticles. The quadratic dependence on the height observed in the experiments is different because it is due to the existence of the stagnation zone. That is why Eq. (B19) does not have a term proportional to h^2 . The stagnation zone is assumed to be constant, independent of the packing density, which remains to be verified. If that is not the case, it adds an extra degree of complexity to the problem.

-
- [1] Y. Tai, L. Wang, G. Yan, J.-m. Gao, H. Yu, and L. Zhang, *Polym. Int.* **60**, 976 (2011).
- [2] U. Lehmann, C. Vandevyver, V. K. Parashar, and M. A. Gijs, *Angew. Chem. Int. Ed.* **45**, 3062 (2006).
- [3] Q. Pankhurst, J. Connolly, S. Jones, and J. Dobson, *J. Phys. D: Appl. Phys.* **36**, R167 (2003).
- [4] A. G. Tibbe, B. G. de Grooth, J. Greve, P. A. Liberti, G. J. Dolan, and L. W. Terstappen, *Nat. Biotechnol.* **17**, 1210 (1999).
- [5] N. Chiannikulchai, Z. Driouich, J. Benoit, A. Parodi, and P. Couvreur, *Sel. Cancer Ther.* **5**, 1 (1989).
- [6] H. Pinto-Alphandary, A. Andremont, and P. Couvreur, *Int. J. Antimicrob. Agents* **13**, 155 (2000).
- [7] B. Teste, F. Kanoufi, S. Descroix, P. Poncet, T. Georgelin, J.-M. Siaugue, J. Petr, A. Varenne, and M.-C. Hennion, *Anal. Bioanal. Chem.* **400**, 3395 (2011).
- [8] S. Cho, S. M. Lee, H. Y. Shin, M. S. Kim, Y. H. Seo, Y. K. Cho, J. Lee, S. P. Lee, and M. I. Kim, *Analyst* **143**, 1182 (2018).
- [9] X. Yu, H.-S. Xia, Z.-D. Sun, Y. Lin, K. Wang, J. Yu, H. Tang, D.-W. Pang, and Z.-L. Zhang, *Biosens. Bioelectron.* **41**, 129 (2013).
- [10] G. Proczek, A.-L. Gassner, J.-M. Busnel, and H. H. Girault, *Anal. Bioanal. Chem.* **402**, 2645 (2012).
- [11] D. Tang, Y. Yu, R. Niessner, M. Miró, and D. Knopp, *Analyst* **135**, 2661 (2010).

- [12] D. Holmes, J. K. She, P. L. Roach, and H. Morgan, *Lab Chip* **7**, 1048 (2007).
- [13] E. Verpoorte, *Lab Chip* **3**, 60N (2003).
- [14] M. A. Gijs, F. Lacharme, and U. Lehmann, *Chem. Rev.* **110**, 1518 (2010).
- [15] G. D. Moeser, K. A. Roach, W. H. Green, T. Alan Hatton, and P. E. Laibinis, *AIChE J.* **50**, 2835 (2004).
- [16] E. P. Furlani and K. C. Ng, *Phys. Rev. E* **73**, 061919 (2006).
- [17] J. Oberteuffer, *IEEE Trans. Magn.* **9**, 303 (1973).
- [18] C. T. Yavuz, J. Mayo, W. Y. William, A. Prakash, J. C. Falkner, S. Yean, L. Cong, H. J. Shipley, A. Kan, M. Tomson *et al.*, *Science* **314**, 964 (2006).
- [19] N. Xia, T. P. Hunt, B. T. Mayers, E. Alsborg, G. M. Whitesides, R. M. Westervelt, and D. E. Ingber, *Biomed. Microdevices* **8**, 299 (2006).
- [20] J. Jung and K.-H. Han, *Appl. Phys. Lett.* **93**, 223902 (2008).
- [21] H. Lee, J. Jung, S.-I. Han, and K.-H. Han, *Lab Chip* **10**, 2764 (2010).
- [22] F. Shen, H. Hwang, Y. K. Hahn, and J.-K. Park, *Anal. Chem.* **84**, 3075 (2012).
- [23] T. Dong, Q. Su, Z. Yang, Y. Zhang, E. B. Egeland, D. D. Gu, P. Calabrese, M. J. Kapiris, F. Karlsen, N. T. Minh *et al.*, *J. Micromech. Microeng.* **20**, 115021 (2010).
- [24] H. Ezzaier, J. A. Marins, S. Schaub, B. H. Amara, and P. Kuzhir, *J. Magn. Magn. Mater.* **459**, 350 (2018).
- [25] G. Orlandi, P. Kuzhir, Y. Izmaylov, J. Alves Marins, H. Ezzaier, L. Robert, F. Doutre, X. Noblin, C. Lomenech, G. Bossis, A. Meunier, G. Sandoz, and A. Zubarev, *Phys. Rev. E* **93**, 062604 (2016).
- [26] B. Teste, F. Malloggi, A.-L. Gassner, T. Georgelin, J.-M. Siaugue, A. Varenne, H. Girault, and S. Descroix, *Lab Chip* **11**, 833 (2011).
- [27] B. Teste, F. Malloggi, J.-M. Siaugue, A. Varenne, F. Kanoufi, and S. Descroix, *Lab Chip* **11**, 4207 (2011).
- [28] P. E. Guevara-Pantoja, M. Sánchez-Domínguez, and G. A. Caballero-Robledo, *Biomicrofluidics* **14**, 014111 (2020).
- [29] P. E. Guevara-Pantoja and G. A. Caballero-Robledo, *RSC Adv.* **5**, 24635 (2015).
- [30] E. Nowak, J. Knight, M. Povinelli, H. Jaeger, and S. Nagel, *Powder Technol.* **94**, 79 (1997).
- [31] J. A. Dijkstra and M. van Hecke, *EPL* **88**, 44001 (2009).
- [32] M. Schröter, D. I. Goldman, and H. L. Swinney, *Phys. Rev. E* **71**, 030301(R) (2005).
- [33] B. Batteiger, W. J. Newhall V, and R. B. Jones, *J. Immunol. Methods* **55**, 297 (1982).
- [34] I. Ogilvie, V. Sieben, C. Floquet, R. Zmijan, M. Mowlem, and H. Morgan, *J. Micromech. Microeng.* **20**, 065016 (2010).
- [35] P. E. Guevara-Pantoja, O. G. Chavez-Pineda, A. M. Solís-Serrano, J. L. García-Cordero, and G. A. Caballero-Robledo, *Lab Chip* **20**, 3179 (2020).
- [36] See Supplemental Material at <http://link.aps.org/supplemental/10.1103/PhysRevE.104.024603> for a schematic representation of the experimental setup and additional data of the experimental protocols.
- [37] G. Gerber, M. Bensouda, D. A. Weitz, and P. Coussot, *Phys. Rev. Lett.* **123**, 158005 (2019).
- [38] J. Jiang, J. Zhan, W. Yue, M. Yang, C. Yi, and C.-W. Li, *RSC Adv.* **5**, 36036 (2015).
- [39] L. Brown, T. Koerner, J. H. Horton, and R. D. Oleschuk, *Lab Chip* **6**, 66 (2006).
- [40] P. E. Guevara-Pantoja, R. J. Jiménez-Valdés, J. L. García-Cordero, and G. A. Caballero-Robledo, *Lab Chip* **18**, 662 (2018).
- [41] D. Ross, M. Gaitan, and L. E. Locascio, *Anal. Chem.* **73**, 4117 (2001).
- [42] T. Aste, M. Saadatfar, and T. J. Senden, *Phys. Rev. E* **71**, 061302 (2005).